Enhancement of the deep-level emission and its chemical origin in hexagonal boron nitride

Tsushima, Emi
Tsujimura, Takuya
Uchino, Takashi

(Citation)
Applied Physics Letters,113(3):031903-031903

(Issue Date)
2018-07-16

(Resource Type)
journal article

(Version)
Version of Record

Enhancement of the deep-level emission and its chemical origin in hexagonal boron nitride

Cite as: Appl. Phys. Lett. **113**, 031903 (2018); https://doi.org/10.1063/1.5038168
Submitted: 02 May 2018 . Accepted: 03 July 2018 . Published Online: 17 July 2018

Emi Tsushima, Takuya Tsujimura, and Takashi Uchino

Enhancement of the deep-level emission and its chemical origin in hexagonal boron nitride

Emi Tsushima, Takuya Tsujimura, and Takashi Uchino
Department of Chemistry, Kobe University, Nada, Kobe 657-8501, Japan

(Received 2 May 2018; accepted 3 July 2018; published online 17 July 2018)

Defect-related deep-level emissions at ∼4 eV from hexagonal boron nitride (h-BN) have been extensively investigated during the past decades. Although the emission has often been associated with deep level impurities such as carbon and oxygen, the structural and chemical origins of the emission center have not yet been identified. Here, we perform systematic photoluminescence measurements and quantitative trace impurity analysis of variously heat-treated h-BN samples with different deep-level emission intensities. In contrast to the common belief, no positive correlation between the impurity (carbon and oxygen) concentration and the deep-level emission intensity was found. We also demonstrate that the intensity of the deep-level emission is significantly enhanced by high-temperature heating (∼1900 °C) under an N_2 environment and subsequent post-annealing at ∼900 °C. These results suggest that intrinsic defects created under N_2-rich conditions are responsible for the deep-level emission. Furthermore, we found that besides the well-recognized zero-phonon line (ZPL) at ∼4.1 eV, additional ZPLs are induced in the near ultraviolet (NUV) region by appropriate annealing of the N_2-treated h-BN sample. The results of temperature-dependent and time-resolved PL measurements on these NUV emission bands are given and discussed. *Published by AIP Publishing*. https://doi.org/10.1063/1.5038168

Hexagonal boron nitride (h-BN) has attracted renewed and growing interest due to its unique structural, electronic and optical properties, such as a graphene-like two-dimensional structure,[1] a wide indirect bandgap of 5.955 eV,[2] and a deep ultraviolet (UV) excitonic emission.[3,4] In addition to these intrinsic properties, defect- and doping-induced properties in h-BN have been under intensive investigation in recent years,[5–9] revealing various interesting properties such as multiband luminescence,[10] insulator-metal transition,[11] single-photon emission,[12–18] ferromagnetism,[19] and catalytic oxygen reduction reaction.[20]

Among all the defect-related phenomena, a deep-level UV emission at ∼4 eV has been widely investigated by experimental and theoretical methods.[10,21–31] The ∼4-eV emission band is composed of regularly spaced sharp peaks, including a zero-phonon line (ZPL) at 4.1 eV[32] and its phonon replicas. In spite of the extensive work performed on this UV emission band, the origin of the defect emission center has not yet been identified. Although carbon and/or oxygen impurities are likely candidates,[27,30,33] there has been no direct experimental proof for this assignment. Recent theoretical investigations have alternatively shown that boron vacancies could be responsible for the ∼4-eV emission.[34]

To shed light on the structural origin of the ∼4-eV emission band in h-BN, we here carry out systematic photoluminescence (PL) measurements and trace elemental analyses for a variety of h-BN samples with different emission intensities. It has been found that there is no correlation between the intensity of the ∼4-eV PL band and the concentration of carbon and oxygen impurities. We also demonstrate that the high-temperature (∼1900 °C) heating under a N_2 atmosphere is especially effective in enhancing the deep-level emission band. These results indicate that the deep-level emission in h-BN results not from extrinsic impurities but from intrinsic defect centers created under N_2-rich conditions. Furthermore, we show that in addition to the well-recognized ZPL at ∼4 eV, spectrally narrow ZPLs can be induced in the near-UV (NUV) region (∼3 eV) by appropriate post-annealing of the N_2-treated h-BN sample.

In this work, we used two types of commercial h-BN powders, which were purchased from Kojundo Kagaku (purity >99%, particle size ∼10 μm) and Aldrich (purity ∼98%, particle size ∼1 μm). In what follows, we will refer to the as-received Kojundo Kagaku and Aldrich h-BN samples as samples K1 and A1, respectively. We confirmed that both the samples show Bragg X-ray diffraction peaks attributed only to the h-BN phase, as shown in Fig. S1 (supplementary material). For details of the experimental procedures, see also Methods in the supplementary material.

Figure 1(a) shows the PL and PL excitation (PLE) spectra of samples K1 and A1 at room temperature. Sample K1 exhibits structured PL and PLE spectra at ∼4 eV, as has often been reported in the literature,[26–30] whereas sample A1 exhibits only a weak UV emission without showing distinct phonon replicas. Since samples K1 and A1 show significantly different deep-level emission characteristics, it is interesting to investigate how the concentration of major impurities in h-BN, i.e., oxygen and carbon, is varied between these two samples. For that purpose, we performed quantitative elemental analysis using high-sensitivity oxygen (LECO, TC-600) and carbon (Horiba, EMIA-920V2) analyzers (for details, see Methods in supplementary material). These quantitative analyses were performed for five different batch samples consisting of ∼1 g for each element. Table I shows the mean (average value) along with a measure of variability. One sees from Table I that both the oxygen and carbon concentrations of sample K1 are almost an order smaller than those of sample A1. It can hence safely be said that the deep-level

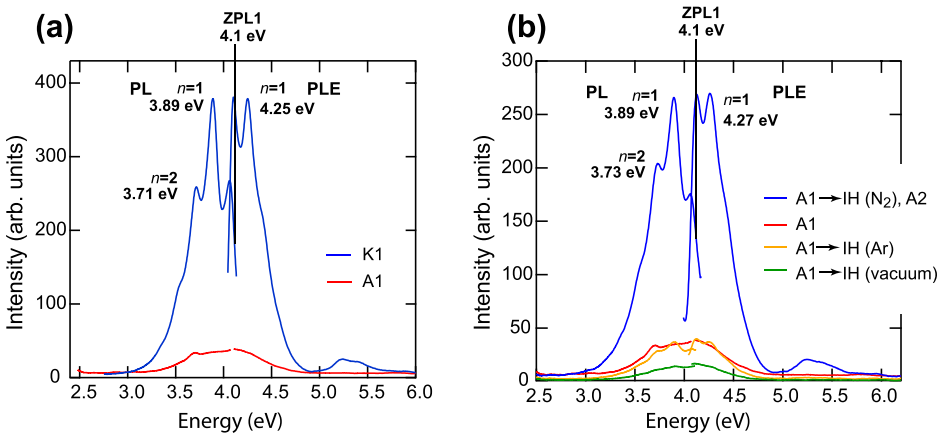

FIG. 1. Room temperature PL and PLE spectra of (a) the as-received Kojundo Kagaku (K1) and Aldrich (A1) samples and (b) the induction heating (IH)-treated A1 samples prepared under different environmental conditions. The PL spectra were recorded with excitation at 4.27 eV and the PLE spectra with emission at 3.89 eV.

TABLE I. Concentration of oxygen and carbon impurities in differently heat-treated h-NB samples.

Sample name	Oxygen (mass %)	Carbon (mass %)
K1	0.11 ± 0.01	0.0043 ± 0.0015
A1	1.6 ± 0.1	0.047 ± 0.002
A2[a]	0.24 ± 0.04	0.053 ± 0.003
A3[b]	0.47 ± 0.01	0.027 ± 0.003

[a]IH heating was carried out for sample A1 under a N_2 atmosphere.
[b]Post-heating was carried out for sample A2 at 900 °C for 3 h under vacuum.

emission, which is substantially enhanced in sample K1 than in sample A1, does not result simply from an oxygen and/or a carbon impurity.

Although the PL intensity of sample A1 is rather low, we found that the intensity of the deep-level PL substantially increases and shows a structured PL band after heating sample A1 at ∼1900 °C for 2 min under a N_2 atmosphere with an induction heating (IH) unit [see Fig. 1(b)]. This N_2-treated A1 sample will be referred to as sample A2. It has been demonstrated that the IH method is quite useful to introduce defect-related emission centers in optically inert high-melting temperature materials such as α-Al_2O_3,[35,36] $MgAl_2O_4$ spinel,[37] AlN,[38] and Mg_3N_2.[39] This is because high temperature IH and successive rapid quenching create and freeze the relevant defect structures in the crystalline lattice. It should, however, be noted that when the IH treatment was carried out under Ar and vacuum, sample A1 does not show an appreciable increase in PL intensity, as shown in Fig. 1(b). We also confirmed that the original crystalline phase of h-BN remains unaffected after IH treatment irrespective of heating environments (see Fig. S1 in supplementary material). Thus, we can conclude that the high-temperature heating under N_2 is especially effective in enhancing the deep-level emission of h-BN. The impurity analysis was also performed for sample A2. As shown in Table I, the concentration of oxygen in sample A2 (∼0.24 wt. %) is quite lower than that in sample A1 (∼1.6 wt. %), whereas that of carbon remained almost unchanged (∼0.05 wt. %) within experimental error between samples A1 and A2. This result is consistent with the above-mentioned result that there is no positive correlation between the intensity of the deep-level emission and the extrinsic impurity concentration. Such an increase in the deep-level PL intensity was also observed for sample K1 after a similar IH treatment (see Fig. S2 in supplementary material); however, the degree of increase is not significant as compared with sample A1.

From these results, it can be deduced that the observed increase in the PL emission intensity, especially of sample A2, after IH treatment in N_2 is induced by

(a) an increase of the density of intrinsic emission centers created under N_2-rich conditions or
(b) a decrease of the density of non-radiative centers during N_2 treatment.

If the mechanism (b) holds, the PL intensity of sample A1 will show a substantial increase at low temperatures, where non-radiative recombination channels will be suppressed. However, the deep-level PL emission of sample A1 remains small even when the temperature is lowered down to 3 K, as shown in Fig. S3 (supplementary material). Thus, mechanism (a) is more likely and intrinsic defects such as N interstitial, B vacancy and/or N antisite, which are expected to be created under N_2-rich conditions,[40,41] are presumably responsible for the deep-level emission at ∼4 eV.

We also found that when sample A2 is post-annealed at temperatures of 700–900 °C, the intensity of the 4.1-eV PL band shows a further increase by a factor of 4–8 irrespective of the annealing gas environment [see, for example, Fig. 2(a)]. On further increase in the post-annealing temperature, the PL intensity was almost saturated. The thus post-annealed sample will be called sample A3. The result of impurity analysis of sample A3 obtained by post-annealing under vacuum conditions is shown in Table I. The carbon concentration of sample A3 is nearly twice smaller than that of sample A2, which is again consistent with our assertion that the carbon impurity is not related to the intensity of the deep-level emission. As for the oxygen impurity, its concentration in sample A3 is almost twice as large as that of sample A2. The slight increase in the oxygen concentration is derived most likely from residual oxygen in the present vacuum (∼30 Pa) heating system. Thus, one might consider that the oxygen impurities can, in part, account for the observed increase in the PL signals. It should, however, be noted that such an increase in the PL emission is not observed when sample A1 is directly annealed in an air atmosphere without N_2 pretreatment (see Fig. S4, supplementary material), indicating that simple (oxidative) annealing will not lead to the enhancement of the deep-level PL intensity. We suggest that

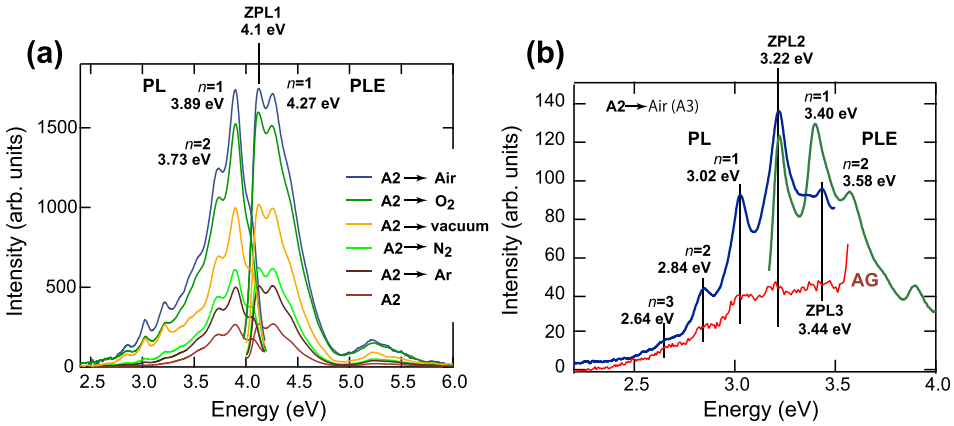

FIG. 2. (a) Room temperature PL and PLE spectra of sample A2 along with those prepared after post-annealing of sample A2 at 900 °C for 3 h under different environmental conditions. (b) Room temperature PL and PLE spectra in the NUV region of sample A3, which was obtained by post-annealing sample A2 in air. In (b), the PL spectrum was recorded with excitation at 3.40 eV and the PLE spectra with emission at 3.02 eV. The bottom curve in (b) shows the room temperature afterglow (AG) spectrum of sample A2 recorded 10 ms after excitation with 3.65-eV light.

the post-annealing process promotes the stabilization (or activation) of the expected intrinsic defect centers created under N_2 treatment, leading to the enhancement of the relevant deep-level emission. This assumption is supported by the observation that the IH-treated K1 sample also shows a significant increase in the deep-level PL intensity after similar post-annealing treatments, as shown in Fig. S2 in supplementary material. The boron vacancy and its related defect complexes are possible candidates for such emission centers because of the two following reasons. First, previous many-body perturbation-theory calculations[34] have shown that among other possible emission centers in h-BN, the best agreement is obtained for the boron vacancy where the main absorption peak of the lower energy regime is at 4.2 eV. Second, it has been theoretically predicted[42] that boron vacancies in the h-BN lattice have several metastable configurations; they can be mobile at temperatures between ~600 and ~1000 °C, leading to vacancy migration and stabilization. We consider that this thermally induced stabilization of boron vacancies can account for the observed enhancement of the deep-level emission shown in Fig. 2(a). That is, non-luminescent centers, which are left in metastable positions, will be converted to luminescent centers by thermal activation. Note, however, that since the resulting PL intensity tends to increase when the post-annealing is carried out under oxidative conditions, such as O_2 and air environments [see Fig. 2(a)], it might also be the case that an oxidative reaction assists, directly or indirectly, the expected thermally induced activation of emission centers.

One also notices from Fig. 2(a) that the post-annealing treatment induces an additional structured PL band in the NUV region below ~3.5 eV. In the following, we will mainly show the results of the sample obtained by post-annealing in air. It should be stressed that this air-annealed sample shows the highest PL intensity among the samples shown in Fig. 2(a), even leading to the maximum internal quantum efficiency of ~50% for the entire emission spectrum. Previously, several researchers[10,21,22,43] also reported the structured emission spectra in the NUV region below ~3.5 eV under excitation with photons of ~4 eV energy (or higher). In these previous works,[10,21] the structured NUV bands were simply interpreted in terms of the higher order phonon replicas of the 4.1-eV ZPL. The PL and PLE spectra of sample A3 in the NUV region [see Fig. 2(b)], however, revealed that the previous interpretation is not valid, as far as the present post-annealed sample is concerned; rather, the PL line at 3.22 eV is attributed to a ZPL since both the PL and PLE spectra yield a common sharp peak at 3.22 eV. In what follows, we refer to the 3.22-eV PL band as ZPL2 to differentiate it from the 4.1-eV ZPL, which will then be called ZPL1. We also notice from Fig. 2(b) that there exist additional sharp peaks, which might result from phonon replicas of ZPL2 or from an unknown ZPL. To clarify this further, we measured the PL spectra of sample A3 at 3 K by changing the excitation energy from ~3 to ~4 eV. Such low-temperature PL measurements are useful to suppress electron-phonon coupling, and hence identify ZPLs and their phonon replicas. The results are given in Fig. 3(a) in the form of a two-dimensional (2-D) PL contour map, and the principal PL and PLE spectra are also shown in Figs. 3(b) and 3(c). The spectral features characteristic to ZPL2 and their phonon replicas are clearly seen, as expected from the results of room-temperature PL measurements. We also notice from Fig. 3 that there exists one more ZPL at 3.44 eV. We will refer to the 3.44-eV ZPL as ZPL3. Since these ZPLs in the NUV region have not been recognized to exist in h-BN previously, we will investigate the NUV emission properties, especially for ZPL2, in more detail.

First, we analyze the PL recombination dynamics of ZPL2 and its photon replicas. Figure 4(a) shows the PL decay profiles of sample A3 in the 2.7–3.2 eV energy range measured at 3 and 300 K under excitation with the second harmonic ($E_{ex} = 3.51$ eV) of a mode locked Ti:Sapphire laser (pulse width: ~180 fs, repetition rate: 8 MHz). It is evident from Fig. 4(a) that the decay profile is temperature insensitive and is characterized by a double exponential function

$$I(t) = I_1 \exp\left(-\frac{t}{\tau_1}\right) + I_2 \exp\left(-\frac{t}{\tau_2}\right), \quad (1)$$

where $I(t)$ is the PL intensity at time t, and I_i and τ_i represent, respectively, the relative initial intensity and the decay time constant of the i-th component. Typical fitted values of τ_i and I_i are as follows: $\tau_1 = 1.7$ ns, $\tau_2 = 3.5$ ns, $I_1 = 0.8$ and $I_2 = 0.2$. The observed two decay time constants suggest the presence of trapping and detrapping processes of the photo-excited electrons via certain trap states during radiative recombination, as has often been observed in trap-related emissions in semiconductors[44] and insulators.[38,45] The temperature independent nature of the decay profile indicates that the excited electronic states are highly localized due to

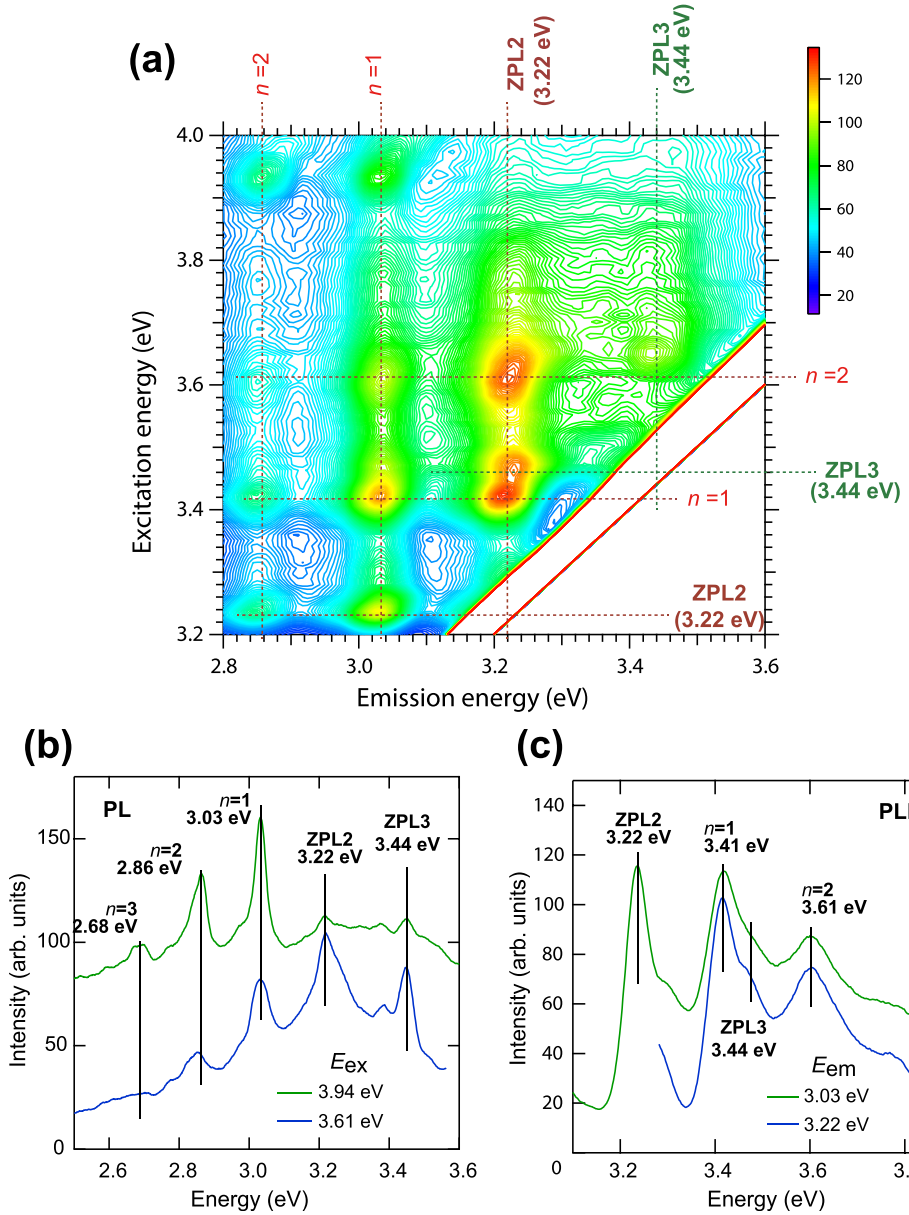

FIG. 3. Low-temperature (3K) PL characteristics of sample A3, which was obtained by post-annealing of sample A2 in air. (a) Contour plot of the PL intensity as a function of excitation and emission energies. (b) 3K PL spectra measured under different excitation energies. (c) 3K PLE spectra measured at different monitor energies.

low electron-phonon coupling and will not compete with any of the nonradiative processes. This is consistent with the observation that the PL intensity in the NUV region (≲3.5 eV) is hardly dependent on temperature (Fig. S5, supplementary material).

In addition to the fast (ns) decay process, we found that sample A3 exhibits weak afterglow (AG) emission in the NUV region especially at temperatures higher than ∼200 K. That is, luminescence persists for ∼10 s after the removal of excitation, as shown in the AG decay curve obtained at room

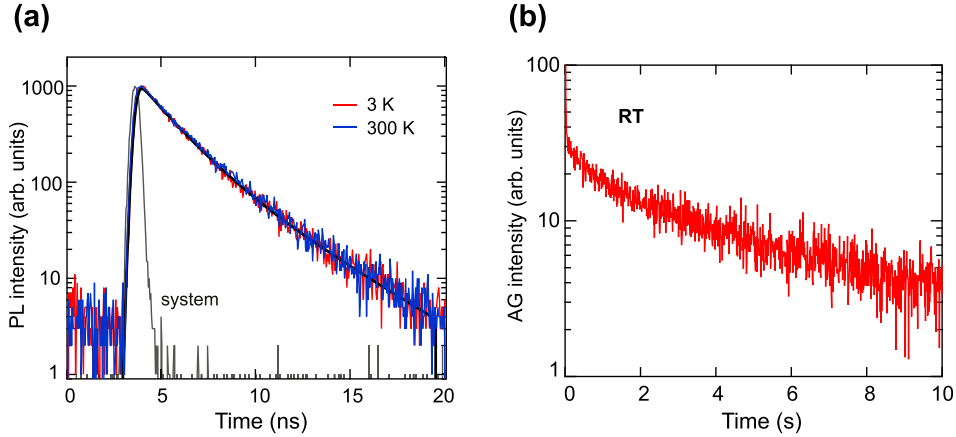

FIG. 4. (a) PL and (b) AG decay profiles of sample A3 in the 2.7–3.2 eV energy region. PL and AG signals were recorded with excitation at 3.5 and 3.6 eV, respectively. The solid line in (a) is the result of fitting to Eq. (1).

temperature [Fig. 4(b)]. This indicates the presence of deep-level traps as the recovery time from deep-level traps could be on the order of seconds or longer depending on the energy level of the trap states. It is also interesting to note that the AG spectrum, which is given in the bottom curve in Fig. 2(b), show structured spectral features, in a similar manner as observed in the PL signals. The peak positions of the AG spectrum coincide well with those of the corresponding PL spectrum, implying that both the PL and AG recombination processes result from the same emission center.

At present, the structural and chemical origins of the deep traps along with those of the NUV emission centers are unknown. However, it is probable that these centers are created during the post-annealing process since the NUV and AG emissions are observed exclusively from Sample A3. It should be noted, however, that the NUV emissions as well as the AG emissions can hardly be observed from sample K1 even after the post-annealing (see Fig. S2 in supplementary material). Since the concentration of carbon in sample K1 is an order smaller than that of sample A series, it is likely that the carbon impurity has a direct or indirect influence on the development of NUV and AG emissions.

In conclusion, we have shown from a systematic impurity analysis of a variety of h-BN samples that there is no correlation between the intensity of the deep-level emission at ~4 eV and the concentration of trace impurities (carbon and oxygen). The intensity of the deep-level PL is increased by high-temperature (~1900 °C) N_2 treatment and then shows a further increase after post-annealing at temperatures of ~900 °C. From the results of the present work and the previous theoretical investigations, we came to a conclusion that boron vacancy is the most likely candidate as the origin of the deep-level emission in h-BN. It has also been found that the post-annealing process results in the well-structured PL emission along with the afterglow emission in the NUV region below ~3.5 eV. There exists at least two ZPLs in the NUV region; one located at 3.22 eV (ZPL2) and the other at 3.24 eV (ZPL3). The relevant emission and charge trapping centers are most likely created during the thermally induced migration of the defects created under N_2-rich conditions, although further work needs to be done to identify the origins of these emission centers.

See supplementary material for more information on experimental methods, XRD patterns and additional PL spectra.

[1]M. Xu, T. L. Minmin, and H. Chen, Chem. Rev. **113**, 3766 (2013).
[2]G. Cassabois, P. Valvin, and B. Gil, Nat. Photonics **10**, 262 (2016).
[3]K. Watanabe, T. Taniguchi, and H. Kanda, Nat. Mater. **3**, 404 (2004).
[4]B. Arnaud, S. Lebègue, P. Rabiller, and M. Alouani, Phys. Rev. Lett. **96**, 026402 (2006).
[5]O. L. Krivanek, M. F. Chisholm, V. Nicolosi, T. J. Pennycook, G. J. Corbin, N. Dellby, M. F. Murfitt, C. S. Own, Z. S. Szilagyi, M. Oxley, S. T. Pantelides, and S. J. Pennycook, Nature **464**, 571 (2010).
[6]D. Wong, J. Velasco, Jr., L. Ju, J. Lee, S. Kahn, H.-Z. Tsai, C. Germany, T. Taniguchi, K. Watanabe, A. Zettl, F. Wang, and M. F. Crommie, Nat. Nanotechnol. **10**, 949 (2015).
[7]Y. Lin, T. V. Williams, W. Cao, H. E. Elsayed-Ali, and J. W. Connell, J. Phys. Chem. C **114**, 17434 (2010).
[8]N. Berseneva, A. Gulans, A. V. Krasheninnikov, and R. M. Nieminen, Phys. Rev. B **87**, 035404 (2013).
[9]M. Gao, M. Adachhi, A. Lyalin, and T. Taketsugu, J. Phys. Chem. C **120**, 15993 (2016).
[10]J. Wu, W.-Q. Han, W. Walukiewicz, J. W. Ager III, W. Shan, E. E. Haller, and A. Zettl, Nano Lett. **4**, 647 (2004).
[11]X. Wei, M.-S. Wang, Y. Bando, and D. Golberg, ACS Nano **5**, 2916 (2011).
[12]T. T. Tran, K. Bray, M. J. Ford, M. Toth, and I. Aharonovich, Nat. Nanotechnol. **11**, 37 (2016).
[13]N. Chejanovsky, M. Rezai, F. Paolucci, Y. Kim, T. Rendler, W. Rouabeh, F. F. de Oliveira, P. Herlinger, A. Denisenko, S. Yang, I. Gerhardt, A. Finkler, J. H. Smet, and J. Wrachtrup, Nano Lett. **16**, 7037 (2016).
[14]T. T. Tran, C. Elbadawi, D. Totonjian, C. J. Lobo, G. Grosso, H. Moon, D. R. Englund, M. J. Ford, J. Aharonovich, and M. Toth, ACS Nano **10**, 7331 (2016).
[15]L. J. Martínez, T. Pelini, V. Waselowski, J. R. Maze, B. Gil, G. Cassabois, and V. Jacques, Phys. Rev. B **94**, 121405(R) (2016).
[16]N. R. Jungwirth and G. D. Fuchs, Phys. Rev. Lett. **119**, 057401 (2017).
[17]G. Grosso, H. Moon, B. Lienhard, S. Ali, D. K. Efetov, M. M. Furchi, P. Jarillo-Herrero, M. J. Ford, I. Aharonovich, and D. Englund, Nat. Commun. **8**, 705 (2017).
[18]R. Bourrellier, S. Meuret, A. Tararan, O. Stéphan, M. Kociak, L. H. G. Tizei, and A. Zobelli, Nano Lett. **16**, 4317 (2016).
[19]Y. Guo and W. Guo, J. Phys. Chem. C **119**, 873 (2015).
[20]J. Zhao and Z. Chen, J. Phys. Chem. C **119**, 26348 (2015).
[21]S. Larach and R. E. Shrader, Phys. Rev. **104**, 68 (1956).
[22]K. Era, F. Minami, and T. Kuzuba, J. Lumin. **24/25**, 71 (1981).
[23]C. A. Tayler II, S. W. Brown, V. Subramaniam, S. Kidner, S. C. Rand, and R. Clarke, Appl. Phys. Lett. **65**, 1251 (1994).
[24]B. Berzina, L. Trinkler, V. Korsak, R. Krutohvostov, D. L. Carroll, K. B. Ucer, and R. T. Williams, Phys. Status Solidi B **243**, 3840 (2006).
[25]P. Jaffrennou, J. Barjon, J.-S. Lauret, B. Attal-Trétout, F. Ducastelle, and A. Loiseau, J. Appl. Phys. **102**, 116102 (2007).
[26]L. Museur, D. Anglos, J.-P. Petitet, J.-P. Michel, and A. V. Kanaev, J. Lumin. **127**, 595 (2007).
[27]T. Taniguchi and K. Watanabe, J. Cryst. Growth **303**, 525 (2007).
[28]M. G. Silly, P. Jaffrennou, J. Barjon, J.-S. Lauret, F. Duastelle, A. Loiseau, E. Obraztsova, and B. Attal-Tretout, Phys. Rev. B **75**, 085205 (2007).
[29]L. Museur, E. Feldbach, and A. Kanaev, Phys. Rev. B **78**, 155204 (2008).
[30]X. Z. Du, J. Li, J. Y. Lin, and H. X. Jiang, Appl. Phys. Lett. **106**, 021110 (2015).
[31]N. L. McDougall, J. G. Partridge, R. J. Nicholls, S. P. Russo, and D. G. McCulloch, Phys. Rev. B **96**, 144106 (2017).
[32]T. Q. P. Vuong, G. Cassabois, P. Valvin, A. Ourghi, Y. Chassagnux, C. Voisin, and B. Gil, Phys. Rev. Lett. **117**, 097402 (2016).
[33]B. Huang and H. Lee, Phys. Rev. B **86**, 245406 (2012).
[34]C. Attaccalite, M. Bockstedte, A. Marini, A. Rubio, and L. Wirtz, Phys. Rev. B **83**, 144115 (2011).
[35]M. Itou, A. Fujiwara, and T. Uchino, J. Phys. Chem. C **113**, 20949 (2009).
[36]S. Ikeda and T. Uchino, J. Phys. Chem. C **118**, 4346 (2014).
[37]S. Sawai and T. Uchino, J. Appl. Phys. **112**, 103523 (2012).
[38]K. Genji and T. Uchino, Appl. Phys. Lett. **109**, 021113 (2016).
[39]Y. Uenaka and T. Uchino, J. Phys. Chem. C **118**, 11895 (2014).
[40]H. Si, G. Lian, A. Wang, D. Cui, M. Zhao, Q. Wang, and C.-P. Wong, Nano Lett. **15**, 8122 (2015).
[41]W. Orellana and H. Chacham, Phys. Rev. B **63**, 125205 (2001).
[42]A. Zobelli, C. P. Ewels, A. Gloter, and G. Seifert, Phys. Rev. B **75**, 094104 (2007).
[43]B. Berzina, V. Korsaks, L. Trinkler, A. Sarakovskis, J. Grube, and S. Bellucci, Diamond Relat. Mater. **68**, 131 (2016).
[44]T. Sauncy, C. P. Palsule, M. Holtz, S. Gangopadhyay, and S. Massie, Phys. Rev. B **53**, 1900 (1996).
[45]N. Sagawa and T. Uchino, Appl. Phys. Lett. **87**, 251923 (2005).